Electronic Supporting Information

Heteroatom-doped hierarchical porous carbons as high-performance metal-free oxygen reduction electrocatalysts

Yun-Pei Zhu,[a] Youlin Liu,[a] Yu-Ping Liu,[a] Tie-Zhen Ren,[b] Gao-Hui Du,[c] Tiehong Chen[a] and Zhong-Yong Yuan[,a]*

[a] *Key Laboratory of Advanced Energy Materials Chemistry (Ministry of Education), Collaborative Innovation Center of Chemical Science and Engineering (Tianjin), College of Chemistry, Nankai University, Tianjin 300071, China. E-mail: zyyuan@nankai.edu.cn.*

[b] *School of Chemical Engineering and Technology, Hebei University of Technology, Tianjin 300130, China.*

[c] *Institute of Physical Chemistry, Zhejiang Normal University, Jinhua 321004, China.*

1. Experimental

1.1 Materials.

1-Hydroxyethylidene-1,1-diphosphonic acid (HEDP), amino trimethylene phosphonic acid (ATMP), and ethylene diamine tetra(methylene phosphonic acid) (EDTMP) were received from Shandong Taihe Chemical Co., Ltd (**Scheme S1**). Methylene diphosphonic acid (MDA), 1,5-naphthalenedisulfonic acid tetrahydrate (1,5-NDA), ethanedisulfonic acid (EDS), 1,3,5-tris(4-carboxyphenyl)benzene (H_3BTB), 2,6-Naphthalenedicarboxylic acid (H_2NDC), were obtained from Sigma-Aldrich Chemical Co (**Scheme S1**). Melamine, dicyandiamide, urea, and boric acid were purchased from Tianjin Guangfu Chemical. All chemicals were used as received without further purification.

1.2 Material preparation.

N,P co-doped porous graphitized carbons (NP-HPC). No templates or surfactants were involved in the entire synthesis. Typically, 6 mmol HEDP and 10 mmol melamine were homogeneously mixed in 50 mL deionized water under vigorous stirring, followed by evaporating the water at 115 ºC. Then, the white samples were further dried at 80 ºC under vacuum conditions for 6h, followed by calcining at 900 ºC for 3h. The ultimate black carbonaceous materials were names as NP-HPC. **N,S co-doped (NS-HPC)** and **N doped (N-HPC)** porous carbons were synthesized in a similar way to NP-HPC, where the sulfonic and carboxylic acids replaced phosphonic acids, respectively.

1.3 Physicochemical characterization.

Scanning electron microscopy (SEM) was carried out on a Jeol JSF-7500L microscope at 5 kV. Transmission electron microscopy (TEM) was carried out on a Jeol JEM 2100F microscope at 200 kV. All samples subjected to TEM measurements were ultrasonically dispersed in ethanol and dropcast onto copper grids covered with a carbon film. Atomic force microscopy (AFM) images were obtained using an SPA-400 atomic force microscope. These probes have a fundamental resonance frequency between 250 and 400 kHz, nominal spring constant of 42 N m^{-1} and nominal tip radius of 10 nm. All images represent flattened data using the NanoScope Analysis version 1.20 software packages. Raman spectra were obtained on Thermo-Fisher Scientific DXR spectrometer

with 532 nm wavelength incident laser light. N_2 adsorption–desorption isotherms were measured on a BELSORP-mini II sorption analyzer at liquid nitrogen temperature (77 K). Prior to measurement, the samples were degassed at 200 ºC overnight. Surface areas were calculated by the multi-point Brunauer–Emmett–Teller (BET) method; total pore volumes were estimated from the volume adsorbed at a relative pressure (P/P_0) of 0.99; the pore-size distribution was calculated from the adsorption branch using the Barrett–Joyner–Halenda (BJH) method. Fourier transform infrared (FT-IR) spectra were measured on a Bruker VECTOR 22 spectrometer with KBr pellet technique, and the ranges of spectrograms were 4000 to 400 cm^{-1}. X-ray diffraction (XRD) patterns were recorded on a Bruker D8 Focus Diffractometer with Cu-K_α radiation (λ = 0.15418 nm) operated at 40 kV and 40 mA. X-ray photoelectron spectroscopy (XPS) measurements were performed on a Kratos Axis Ultra DLD (delay line detector) spectrometer equipped with a monochromatic Al-K_α X-ray source (1486.6 eV). All XPS spectra were recorded using an aperture slot of 300 × 700 microns, survey spectra were recorded with a pass energy of 160 eV and high resolution spectra with a pass energy of 40 eV. Thermogravimetry analysis (TGA) was performed using a TA SDT Q600 instrument at a heating rate of 10 ºC min^{-1} using α-Al_2O_3 as the reference.

1.4 Electrode preparation and electrocatalytic activity evolution.

In order to prepare the working electrode, 4 mg of NPMC samples were dispersed in an aqueous solution containing 0.5 mL Mill-Q water and 0. 5 mL isopropanol under sonication. The glass carbon (GC) electrode (5 mm in diameter) was firstly polished with 0.5 μm down to 0.05 μm alumina powder, washed with Mill-Q water and ethanol and allowed to dry. 10 μL of the obtained homogeneous catalyst ink was dropped onto the mirror polished glassy carbon electrode. Following overnight solvent evaporation in air, a thin layer of Nafion® solution was coated onto the electrode surface and then dried in air for 1 h; the resulting electrode served as a working electrode. All the electrochemical measurements were conducted in a three-electrode configuration. Ag/AgCl was used as the reference electrode and the counter electrode was platinum wire. Pt/C (20 wt%, Alfa Aesar) electrode was prepared by using the same procedure. Electrochemical experiments were conducted at room temperature on a CHI660D electrochemical workstation (CH instrument Co. USA).

A flow of O_2 was maintained over the electrolyte (0.1 M KOH) during the recording of

electrochemical measurements in order to ensure its continued O_2 saturation. Cyclic voltammograms (CVs) and linear sweep voltammograms (LSVs) were carried out using a glassy carbon RDE. The scan rate of CVs was kept as 20 mV s^{-1} while that for LSVs was 10 mV $^{-1}$. All the electrochemical data were recorded after contiguous CV cyclic scans at a rate of 20 mV s^{-1} for at least 20 times. On the basis of RDE data, the overall electron transfer number per oxygen molecule involved in oxygen reduction can be determined by Koutechy-Levich (K-L) equation:[S1,S2]

$$1/J = 1/J_k + 1/J_L = 1/J_k + 1/B\omega^{1/2} \quad (1)$$

where J_k is the kinetic current and ω is the electrode rotating rate. B is determined from the slope of the K-L plots based on the Levich equation as given below:

$$B = 0.2nF(D_{O2})^{2/3}\upsilon^{-1/6}C_{O2} \quad (2)$$

where n represents the transferred electron number per oxygen molecule. F is Faraday constant (F = 96485 C mol^{-1}). D_{O2} is the diffusion coefficient of O_2 in 0.1 M KOH (D_{O2} = 1.9 × 10^{-5} cm^2 s^{-1}). υ is the kinetic viscosity (υ = 0.01 cm^2 s^{-1}). C_{O2} is the bulk concentration of O_2 (C_{O2} = 1.2 × 10^{-6} mol cm^{-3}). The constant 0.2 is adopted when the rotation speed is expressed in rpm. For the Tafel plot, the kinetic current was calculated from the mass-transport correction of RDE using the following equation:

$$J_k = J \times J_L/(J_L - J) \quad (3)$$

2. Supplementary figures

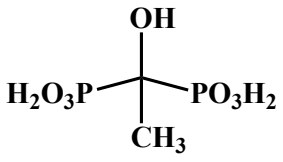

HEDP

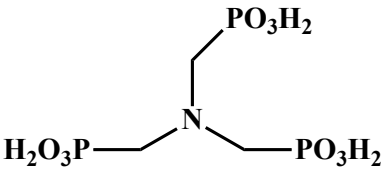

ATMP

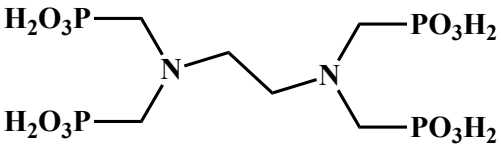

EDTMP

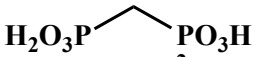

MDP

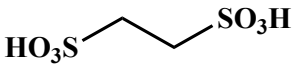

EDS

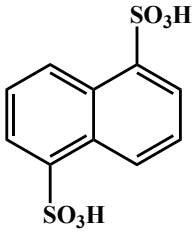

1,5-NDA

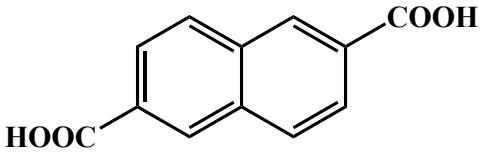

H_2NDC

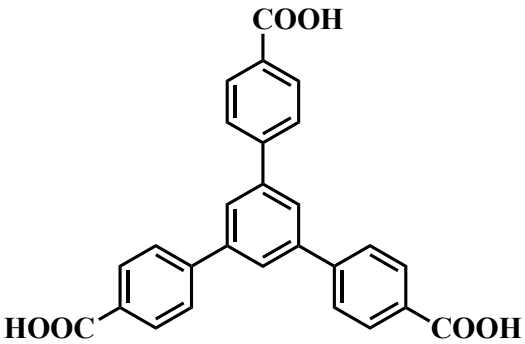

H_3BTB

Scheme S1. Structural formulas of the used phosphonic, sulfonic, and carboxylic acids.

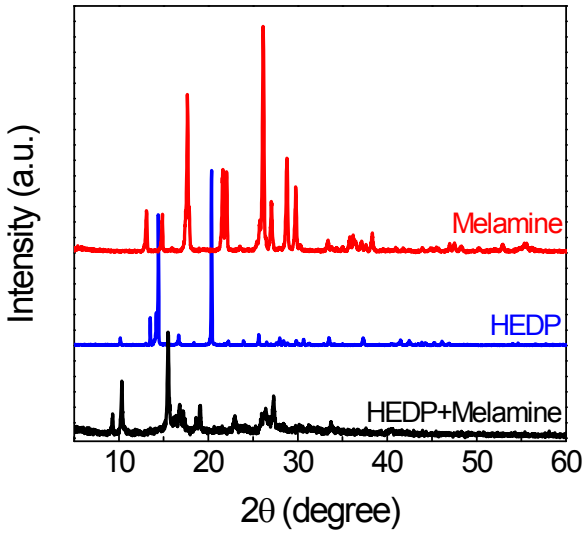

Fig. S1 XRD patterns of melamine, HEDP, and the corresponding mixtures (HEDP+Melamine).

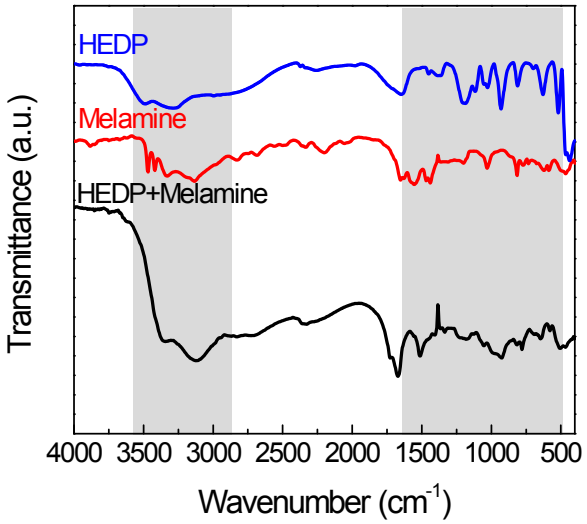

Fig. S2 FT-IR spectra patterns of melamine, HEDP, and the corresponding mixtures. The gray areas present the vibration bands of typical HEDP and melamine. For HEDP, the sharp band around 930 cm^{-1} is related to P–OH and the shoulder band at about 1450 cm^{-1} is corresponded to P–C stretching vibration.[S3] As to melamine, the bands around 3450 cm^{-1} are assigned to $–NH_2$ [S4] and the band at 820 cm^{-1} is related to stretching vibrations of triazine ring[S5]. With respect to the polymer form HEDP and melamine (HEDP + Melamine), the bands attributed to P–OH and $–NH_2$ weaken or disappear, which accompanies by the preservation of typical P–C band and vibrations of triazine ring, implying the formation of polymers via acid-base interaction.

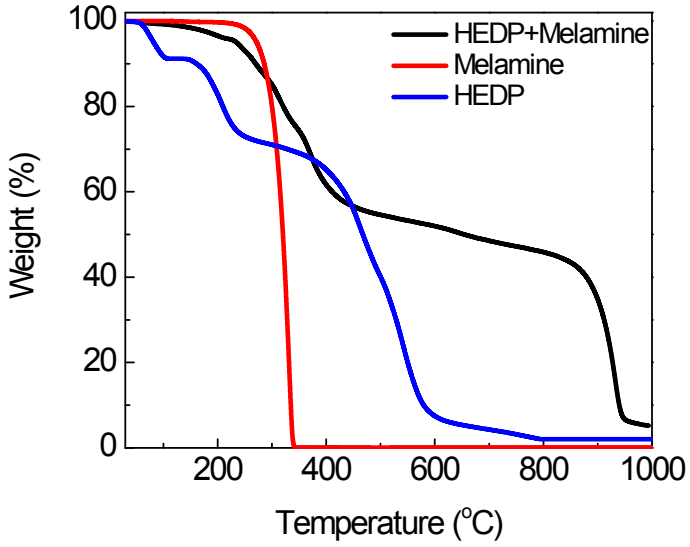

Fig. S3 TGA curves of melamine, HEDP, and the corresponding mixtures. For the polymer, the weight loss from room temperature to 180 ºC is due to the desorption of water molecules. The second stage in the range of 180–600 ºC is attributed to the decomposition of organics, and the last weight loss above 600 ºC can be related to deep carbonization process and loss of volatiles.

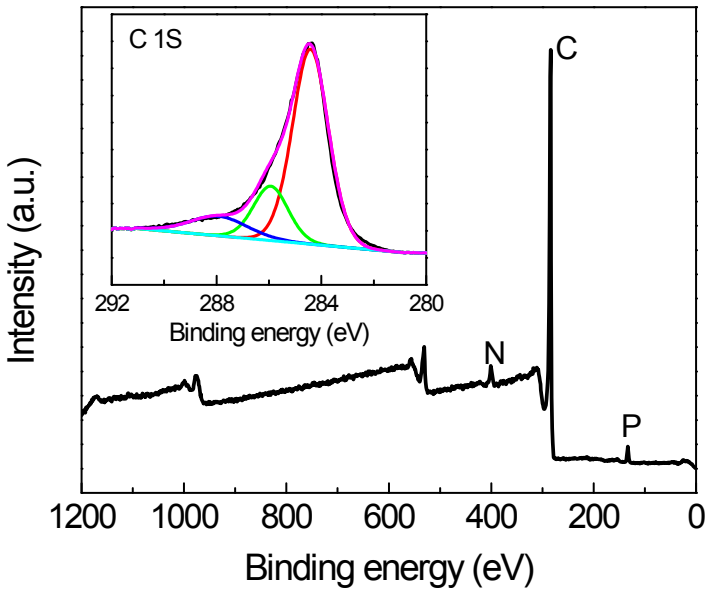

Figure S4. XPS survey and high-resolution spectra of C 1s core levels in NC-HPC.

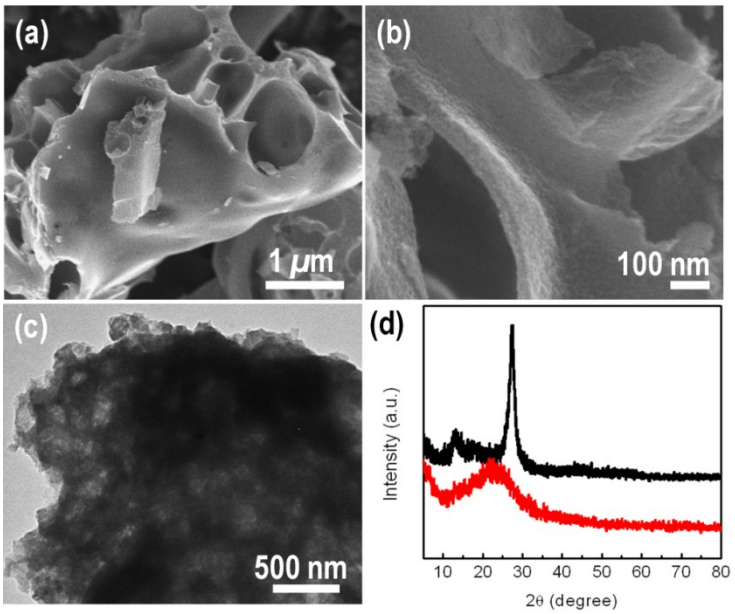

Fig. S5 SEM (a, b) and TEM (c) images of the carbonaceous materials obtained by calcination of the HEDP-melamine induced polymers at 550 ºC for 4 h (denoted as NP-PC-550). (d) Power XRD patterns of the NP-PC-500-4 (red solid line) and graphitic carbon nitride (g-C_3N_4, black solid line).

Fig. S5a-c show the formation of porosity and thick layers. It should be noted that calcination of single melamine at 550 ºC for 4h leads to the formation of g-C_3N_4, showing two characteristic peaks at 2θ = 13.8 º and 27.3º.[S6] However, NP-PC-550 exhibit no typical diffractions attributable to g-C_3N_4, indicating that the intimate interaction between acid and base units generates stable polymer and the pyrolysis and carbonization processes occur during the increase of temperature.

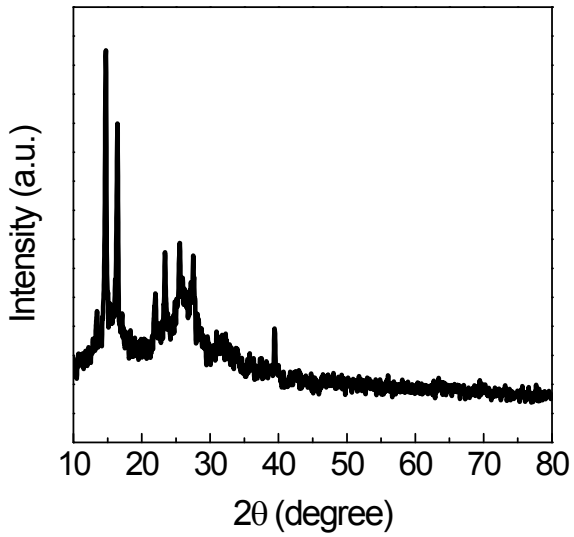

Fig. S6 XRD pattern of the yellow-red solid deposited on the furnace walls, which could be assigned to elemental phosphorus.

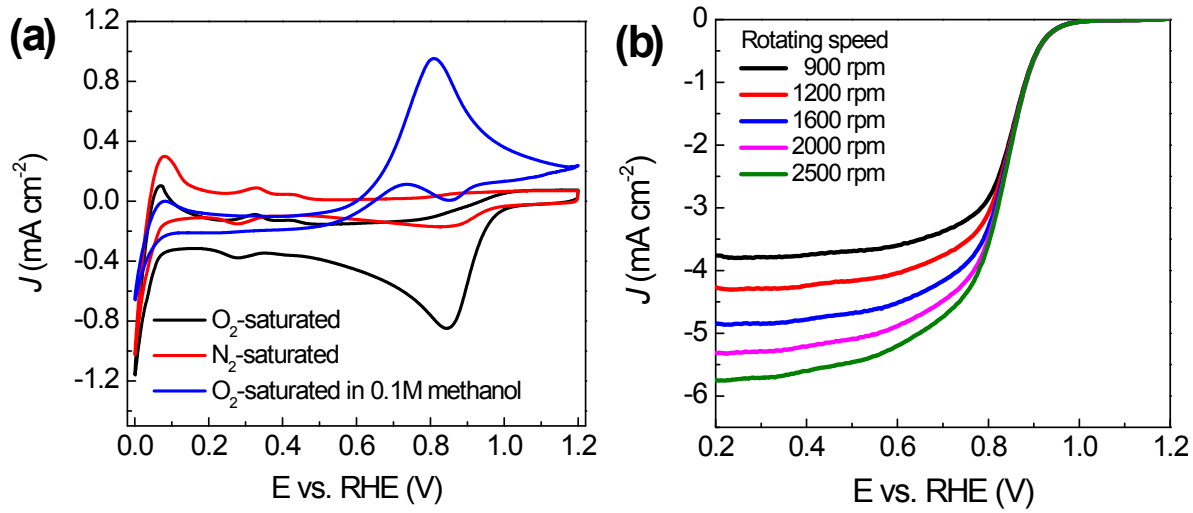

Fig. S7 (a) CV curves of commercial Pt/C in N_2-saturated 0.1 M KOH, O_2-saturated 0.1 M KOH, and O_2-saturated 1 M methanol solutions. Scan rate: 20 mV s^{-1}. (b) ORR polarization curves of Pt/C at different rotating speeds.

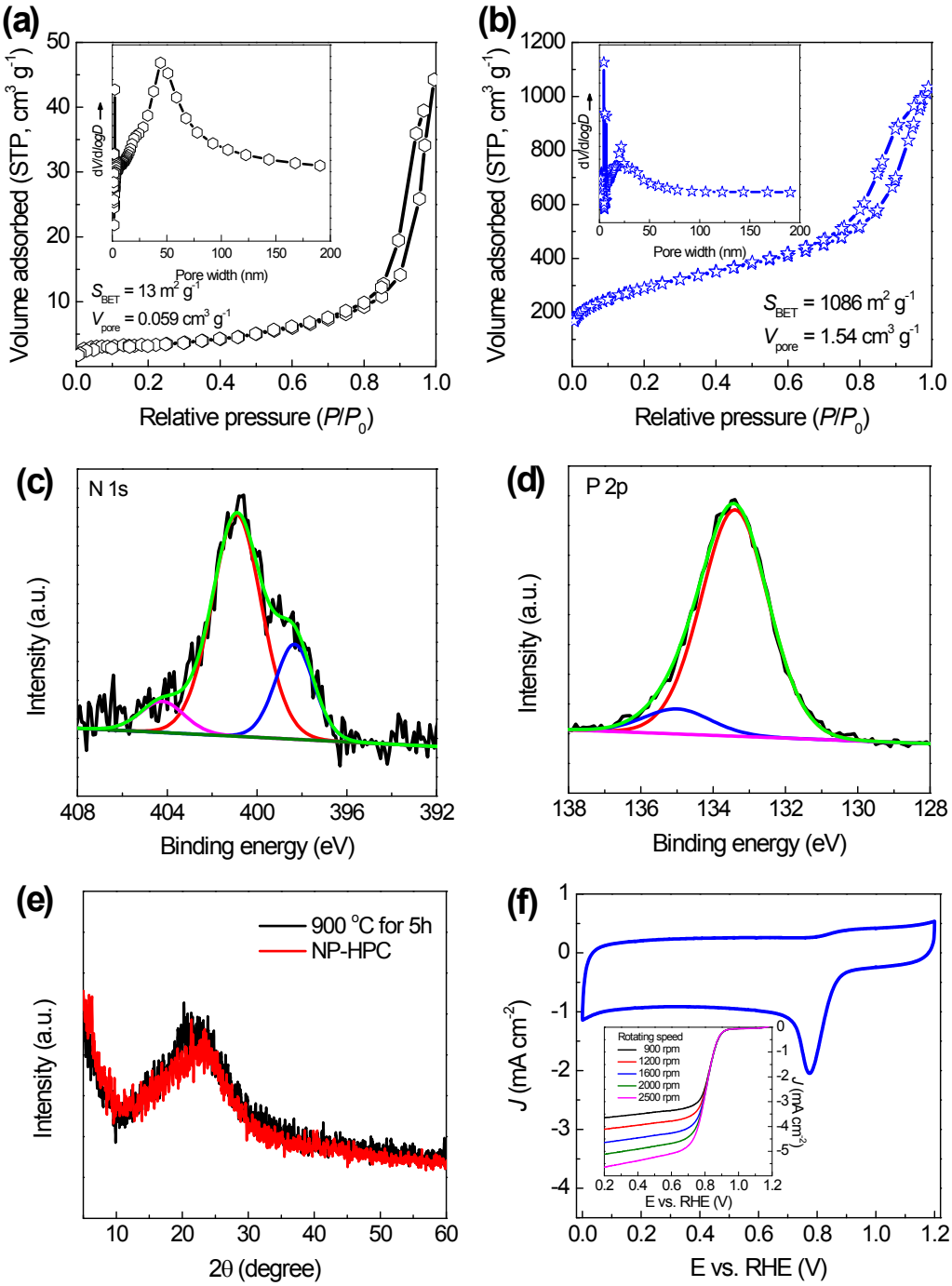

Fig. S8 N_2 sorption isotherm of the samples prepared via calcining at 800 ºC for 3h (a) and 900 ºC for 5h (b), respectively. Inset: pore size distribution curves. (c, d) High-resolution N 1s and P 2p XPS spectra in the sample via calcining at 900 ºC for 5h. (e) Comparison of the XRD patterns. (f) the corresponding CV curve in O_2-saturated 0.1 M KOH at a sweep rate of 20 mV s^{-1}. Inset: ORR polarization curves at different rotating speeds at a sweep rate of 10 mV s^{-1}. The N and P atomic content based on XPS are determined to be 1.84 and 1.49 at%, respectively. The increased intensity of XRD diffraction peak reveals the increase of graphitization degree. The lower surface area and heteroatom contents can be related to increased graphitic and stacking degree.

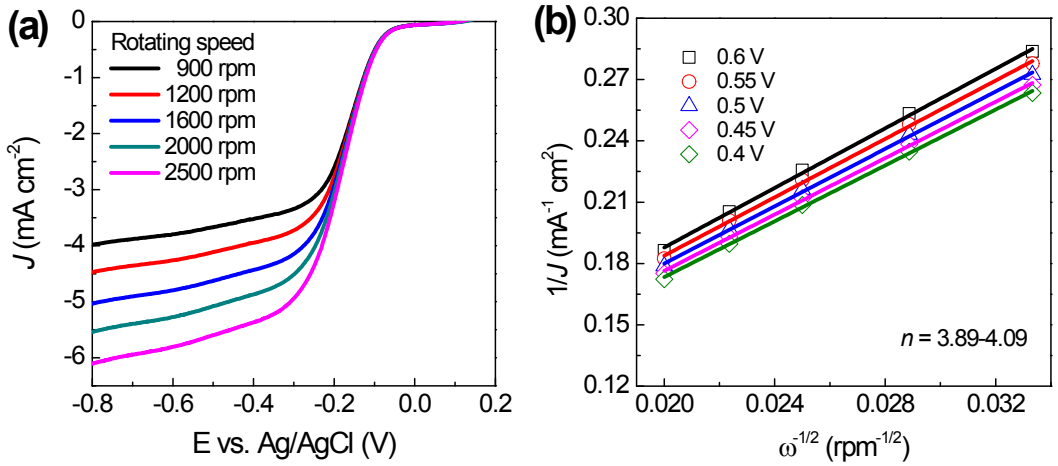

Fig. S9 (a) ORR polarization curves of NP-HPC at different rotating speeds in an O_2-saturated 0.1 M KOH aqueous solution. (b) The corresponding K-L plots at various potentials, indicating the pseudo-four-electron ORR process in a wide potential range.

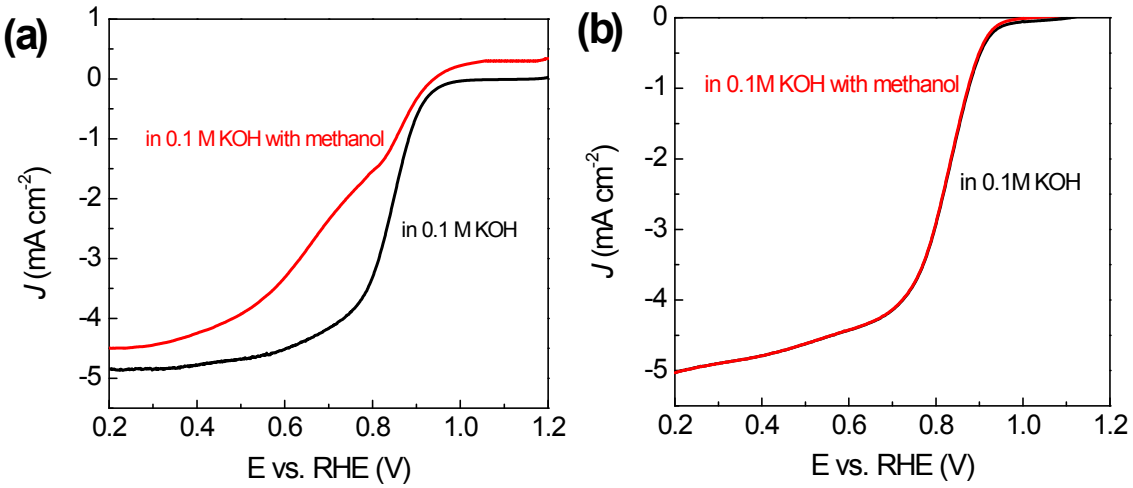

Fig. S10 Liner sweep voltammograms on RDE for (a) Pt/C electrode and (b) NP-HPC electrode in O_2-saturated 0.1 M KOH and with 1 M methanol at a rotating speed of 1600 rpm. The ORR curve for Pt/C electrode shows a weak oxidation peak between 0.8 V in the presence of methanol, which could be ascribed to the oxidation of methanol. In addition, Pt/C electrode shows a negative on-set potential shift for ORR with the addition of methanol. On the contrary, no significant difference and/or changes of the ORR curves can be detected for the NP-HPC electrocatalyst in the presence of methanol.

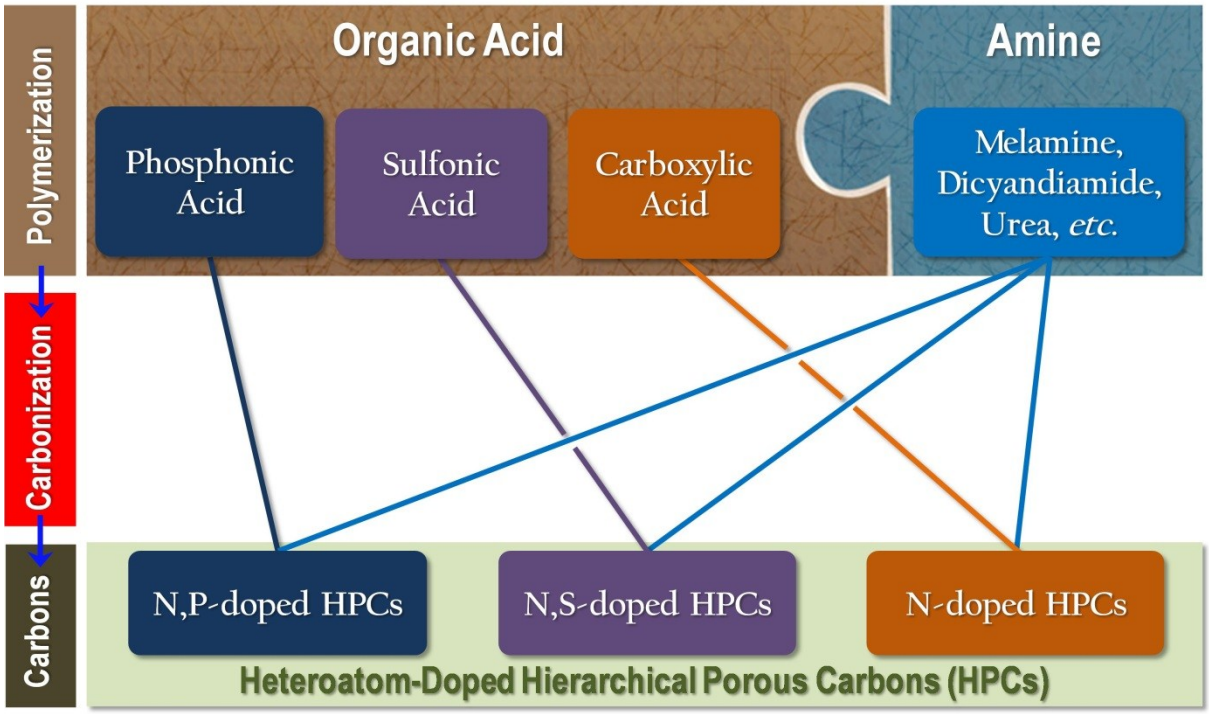

Fig. S11 General scheme of the acid-amine polymerization-carbonization strategy for heteroatom-doped HPCs.

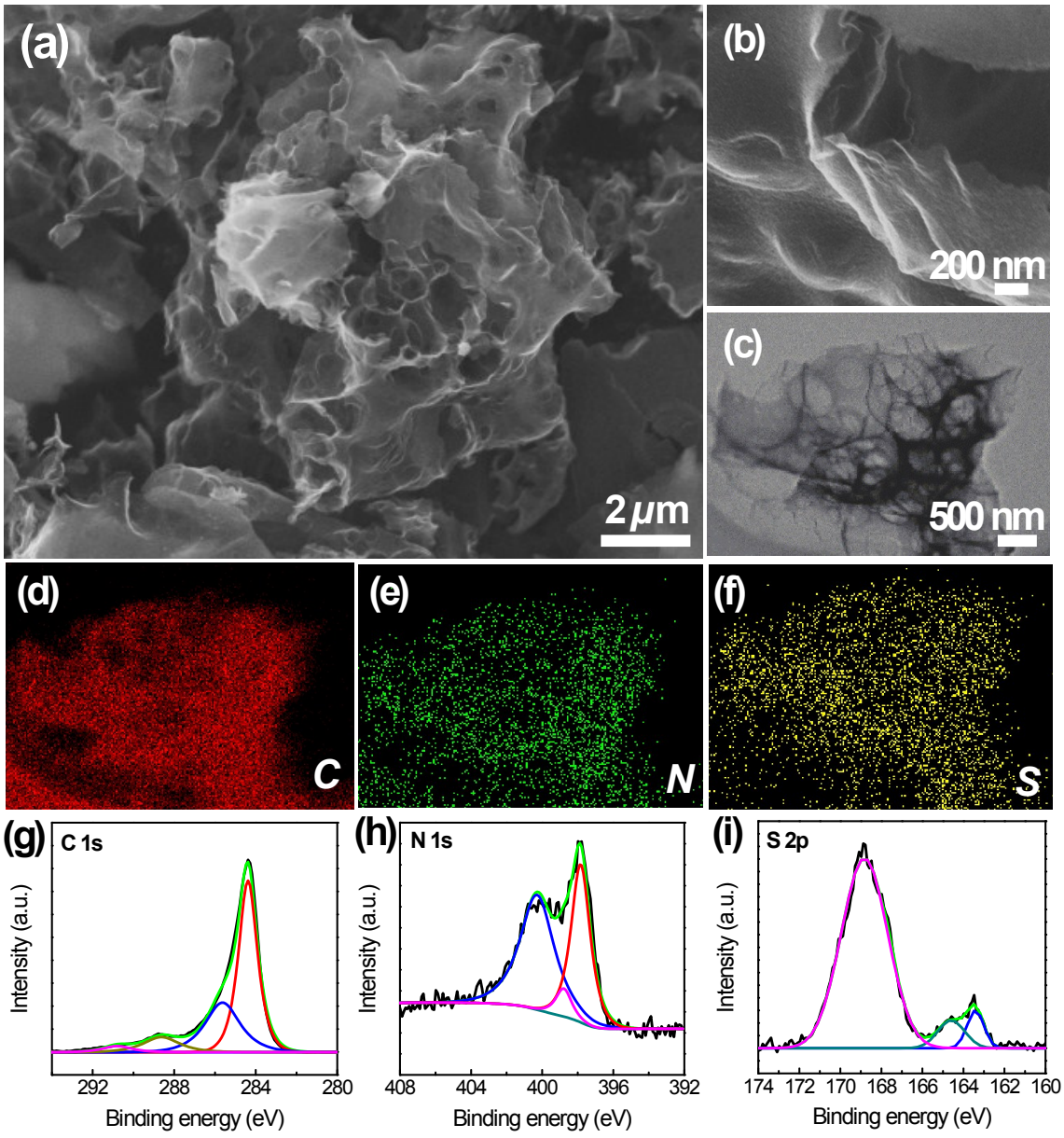

Fig. S12 SEM (a, b) and TEM (c) images of NS-HPC synthesize by using melamine and H_3BTB, and the corresponding EDX elemental mapping (d-f). High-resolution XPS spectra of C 1s (g), N1s (h), and S 2p (i). Analysis of N 1s spectra reveals the presence of pyridinic N and quaternary N, ascribing to binding energies of 398.7 and 401.1 eV, respectively. As to the S 2p fine spectra, three different peaks at 168.7, 164.5, and 163.4 eV can be resolved. The prominent contribution at higher binding energy of 168.7 eV is attributable to the sulfate groups (–C–SO_x–C–, x = 2–4); the peak at 163.4 eV for S $2p_{3/2}$ and the peak at 164.5 eV for S $2p_{1/2}$ correspond to thiophene-S groups (–C–S–C–).[S7] The atomic ratios of N and S based on XPS analysis are determined to be 3.76% and 4.24%, respectively.

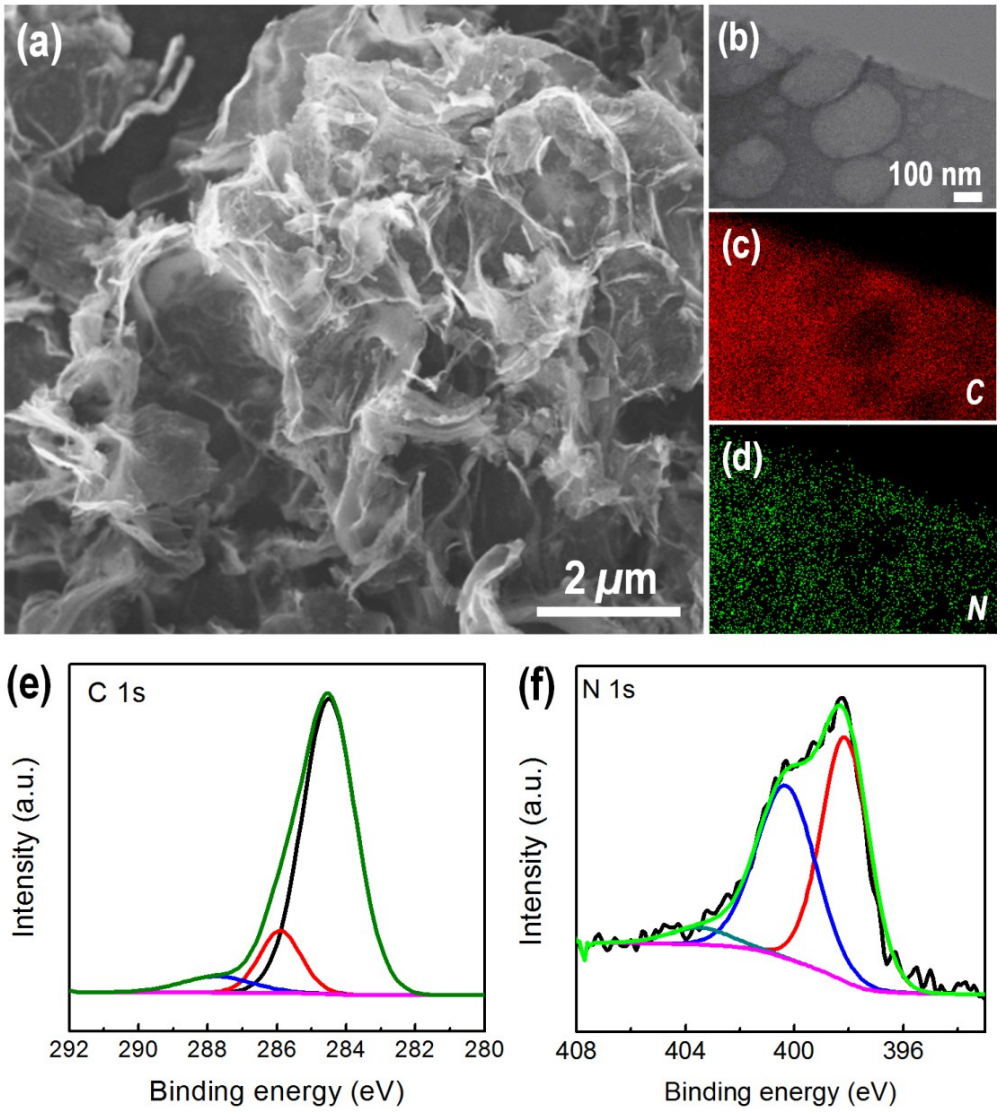

Fig. S13 SEM (a) and TEM (b) images of N-HPC synthesized by using melamine and 1,5-NDA, and the corresponding EDX elemental mapping (c, d). High-resolution XPS spectra of C 1s (e) and N 1s (f). The N atomic content according to XPS characterization is determined to be 5.36%.

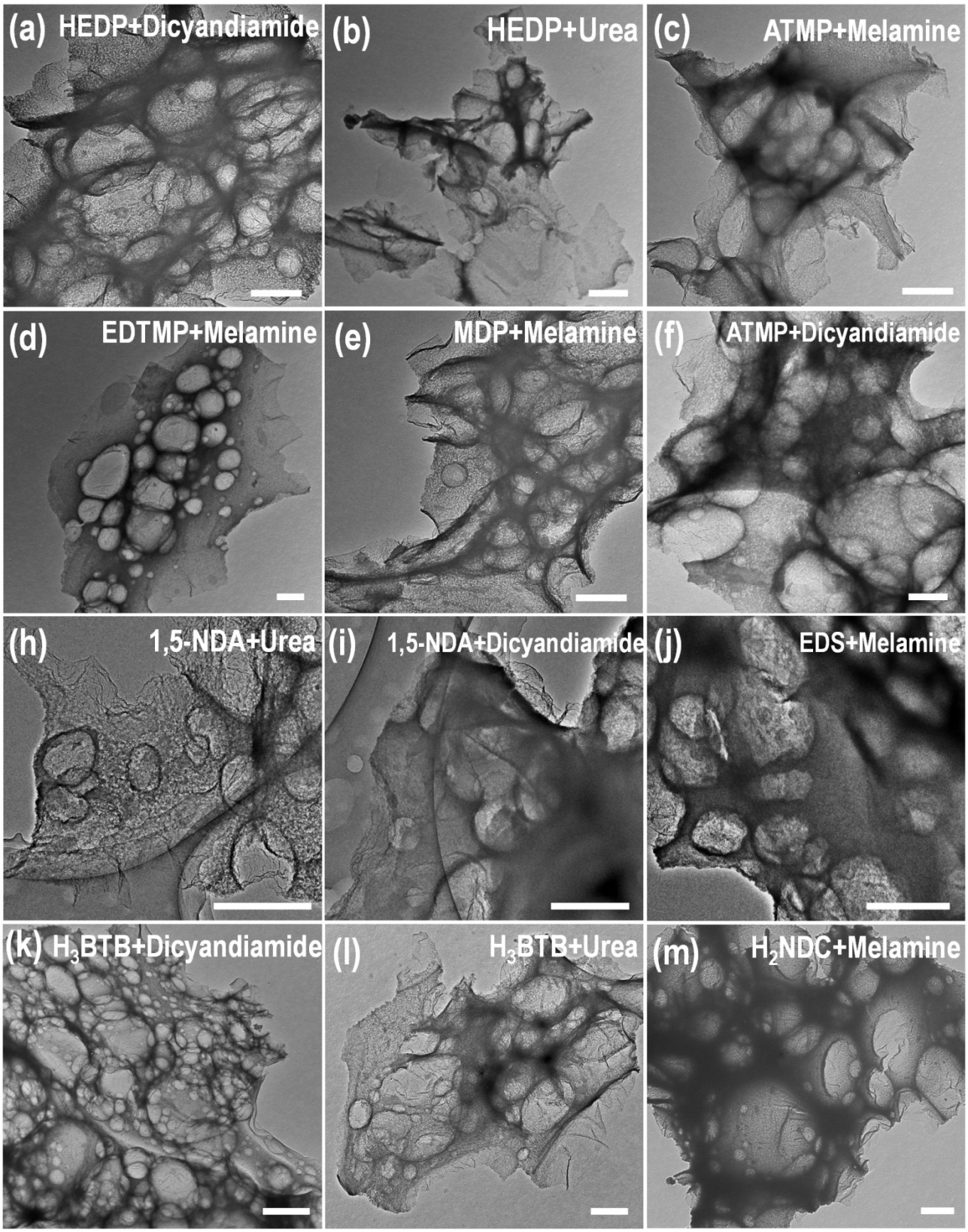

Fig. S14 TEM images of porous carbon materials through the combination of different organic acids and bases. **Scale Bar: 500 nm**.

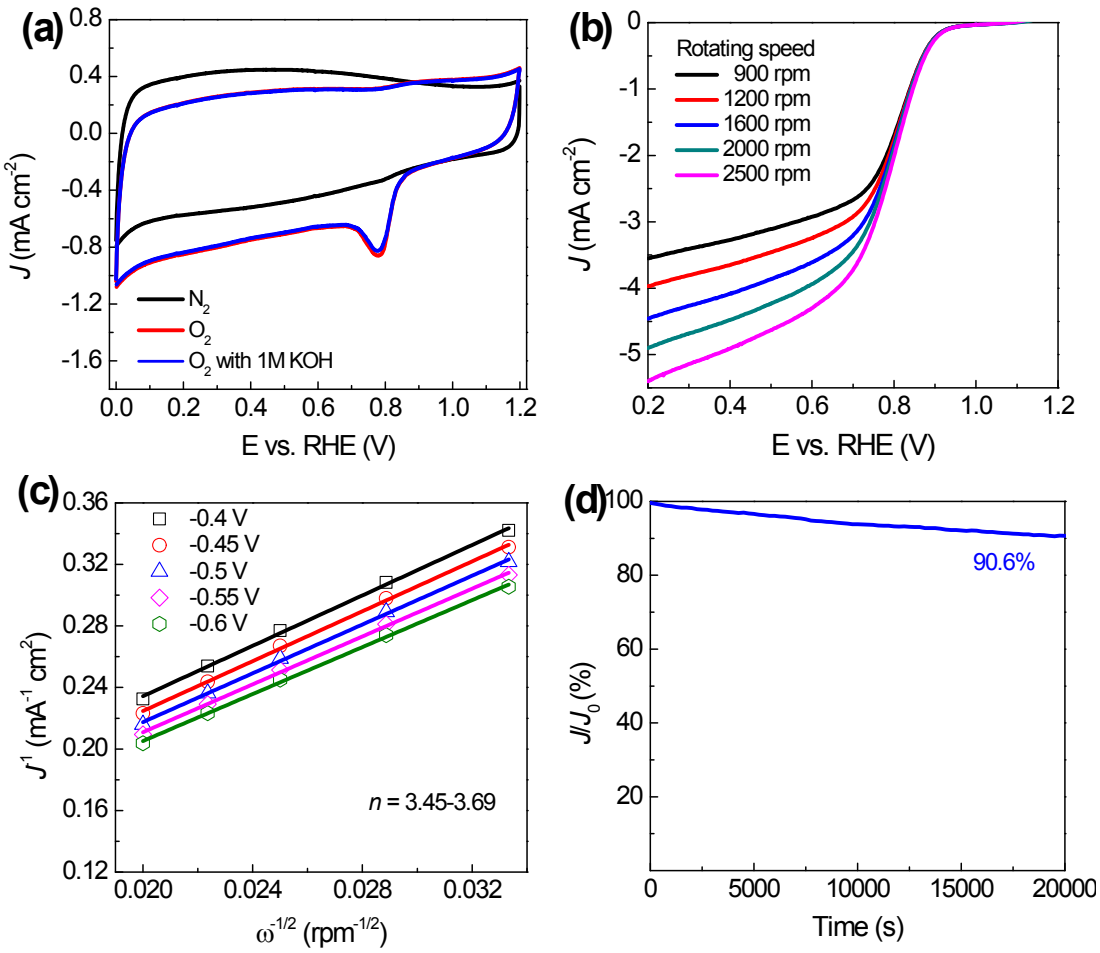

Fig. S15 (a) CV curves of NS-HPC in N_2-saturated 0.1 M KOH, O_2-saturated 0.1 M KOH, and O_2-saturated 1 M methanol solutions. Scan rate: 20 mV s^{-1}. (b) Liner sweep voltammograms in O_2-saturated 0.1 M KOH at a scan rate of 10 mV s^{-1} at 1600 rpm. (c) K-L plots at different potentials. (d) The chronoamperometric response curve at 0.6 V.

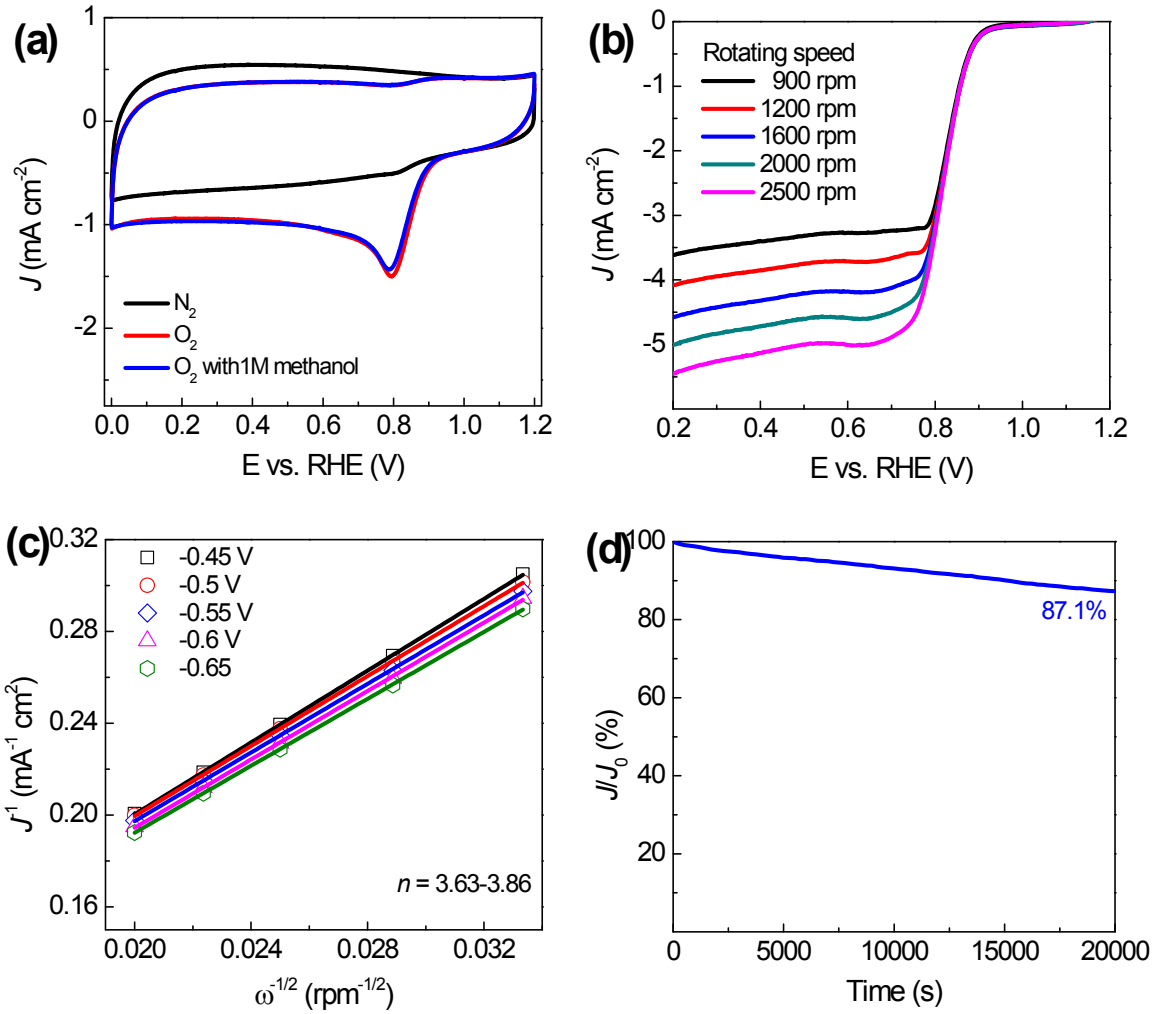

Fig. S16 (a) CV curves of N-HPC in N_2-saturated 0.1 M KOH, O_2-saturated 0.1 M KOH, and O_2-saturated 1 M methanol solutions. Scan rate: 20 mV s^{-1}. (b) Liner sweep voltammograms in O_2-saturated 0.1 M KOH at a scan rate of 10 mV s^{-1} at 1600 rpm. (c) K-L plots at different potentials. (d) The chronoamperometric response curve at 0.6 V.

Table S1. Comparison of ORR catalytic performances between NP-HPC and previously reported chemically modified carbon materials in 0.1 M KOH.

Catalyst	Surface area ($m^2\ g^{-1}$)	Onset potential (V, vs. RHE)	ORR peak potential (V, vs. RHE)	Catalyst loading ($mg\ cm^{-2}$)	Half-wave potential (V, vs. RHE)	Ref.
NP-HPC	**1283**	**0.949**	**0.822**	**0.204**	**0.83**	**This work**
Mesoporous N-doped carbons	1553	1.01	0.781	0.803	N.A.	S8
N,S,O-doped nanoporous carbons	1180	-0.012	0.753	0.203	0.74	S9
KOH activated N-doped carbons	2191	0.961	0.805	0.077	0.83	S10
N,B-doped graphene	N.A.	1.03	0.693	0.283	N.A.	S11
P-doped ordered mesoporous carbons	1182	0.863	0.783	0.79	N.A.	S12
N,O-doped mesoporous carbons	32.4	0.71	N.A.	0.1	N.A.	S13
Hierarchical porous NPCs	756	0.943	0.663	0.102	N.A.	S14
ZIF derived N-doped carbons	519	0.915	0.769	0.2	N.A.	S15
N-doped graphene QDs	N.A.	0.81	0.703	0.28	N.A.	S16
Graphene-based carbon nitride	542	N.A.	0.723	0.071	N.A.	S17
P-doped graphene	N.A.	0.92	0.561	0.051	N.A.	S18
N-OMMC-G	1121	0.923	0.693	0.41	N.A.	S19
N,S-doped carbon aerogels	225	0.843	0.603	0.28	N.A.	S20
CNT/HDC-1000	3325	N.A.	N.A.	N.A.	0.82	S21
VA-NCNT film	N.A.	N.A.	N.A.	N.A.	0.788	S22
Hierarchally porous N-doped carbon	1280	N.A.	N.A.	0.1	0.85	S23

Supplementary References

S1 S. H. Oh, R. Black, E. Pomerantseva, J. H. Lee, L. F. Nazar, *Nat. Chem.* **2012**, *4*, 1004–1010.

S2 Y. Liang, Y. Li, H. Wang, J. Zhou, J. Wang, T. Regier, H. Dai, *Nat. Mater.* **2011**, *10*, 780–786.

S3 T. Y. Ma, X. Z. Lin, Z. Y. Yuan, *Chem. Eur. J.* **2010**, *16*, 8487–8494.

S4 H. Li, T. Y. Ma, D. M. Kong, Z. Y. Yuan, *Analyst* **2013**, *138*, 1084–1090.

S5 Y. P. Zhu, M. Li, Y. L. Liu, T. Z. Ren, Z. Y. Yuan, *J. Phys. Chem. C* **2014**, *118*, 10963–10971.

S6 J.Zhang, F. Guo, X. Wang, *Adv. Funct. Mater.* **2013**, *23*, 3008–3014.

S7 X. Chen, X. Chen, X. Xu, Z. Yang, Z. Liu, L. Zhang, X. Xu, Y. Chen, S. Huang, *Nanoscale* **2014**, *6*, 13740–13747.

S8 W. Yang, T. P. Fellinger, M. Antonietti, *J. Am. Chem. Soc.* **2011**, *133*, 206–209.

S9 Y. Meng, D. Voiry, A. Goswami, X. Zou, X. Huang, M. Chhowalla, Z. Liu, T. Asefa, *J. Am. Chem. Soc.* **2014**, *136*, 13554−13557.

S10 W. He, C. Jiang, J. Wang, L. Lu, *Angew. Chem. Int. Ed.* **2014**, *53*, 9503–9507.

S11 Y. Zheng, Y. Jiao, L. Ge, M. Jaroniec, S. Z. Qiao, *Angew. Chem. Int. Ed.* **2013**, *52*, 3110–3116.

S12 D. S. Yang, D. Bhattacharjya, S. Inamdar, J. Park and J. S. Yu, *J. Am. Chem. Soc* **2012**, *134*, 16127–16120.

S13 R. Silva, D. Voiry, M. Chhowalla and T. Asefa, *J. Am. Chem. Soc.*, **2013**, *135*, 7823–7826.

S14 H. Jiang, Y. Zhu, Q. Feng, Y. Su, X. Yang and C. Li, *Chem. Eur. J.* **2014**, *20*, 3106–3112.

S15 H. X. Zhong, J. Wang, Y. W. Zhang, W. L. Xu, W. Xing, D. Xu, Y. F. Zhang and X. B. Zhang, *Angew. Chem. Int. Ed.* **2014**, *53*, 14235–14239.

S16 Y. Li, Y. Zhao, H. Cheng, Y. Hu, G. Shi, L. Dai and L. Qu, *J. Am. Chem. Soc.* **2012**, *134*, 15–18.

S17 S. Yang, X. Feng, X. Wang, and K. Müllen, *Angew. Chem. Int. Ed.* **2011**, *50*, 5339–5343.

S18 C. Zhang, N. Mahmood, H. Yin, F. Liu and Y. Hou, *Adv. Mater.* **2013**, *25*, 4932–4937.

S19 J. Liang, X. Du, C. Gibson, X. W. Du and S. Z. Qiao, *Adv. Mater.* **2013**, *25*, 6226–6231.

S20 S. A.Wohlgemuth, R. J. White, M. G. Willinger, M. M. Titiricia and M. Antonietti, *Green Chem.* **2012**, *14*, 1515–1523.

S21 Y. J Sa, C. Park, H. Y. Jeong, S. H. Park, Z. Lee, K. T. Kim, G. G. Park and S. H. Joo, *Angew. Chem., Int. Ed.* **2014**, *53*, 4102–4106.

S22 K. Gong, F. Du, Z. Xia, M. Durstock, L. Dai, *Science* **2009**, *323*, 760–764.

S23 H. W. Liang, X. Zhuang, S. Brüller, X. Feng and K. Müllen, *Nat. Commun.* **2014**, *5*, 4973.